Vol 453|15 May 2008|doi:10.1038/nature06868

LETTERS

Vascular normalization in *Rgs5*-deficient tumours promotes immune destruction

Juliana Hamzah[1], Manfred Jugold[2], Fabian Kiessling[2], Paul Rigby[5], Mitali Manzur[1], Hugo H. Marti[6], Tamer Rabie[6], Sylvia Kaden[3], Hermann-Josef Gröne[3], Günter J. Hämmerling[4], Bernd Arnold[4] & Ruth Ganss[1]

The vasculature of solid tumours is morphologically aberrant and characterized by dilated and fragile vessels, intensive vessel sprouting and loss of hierarchical architecture[1]. Constant vessel remodelling leads to spontaneous haemorrhages[2] and increased interstitial fluid pressure in the tumour environment[3,4]. Tumour-related angiogenesis supports tumour growth and is also a major obstacle for successful immune therapy as it prevents migration of immune effector cells into established tumour parenchyma[2,5,6]. The molecular mechanisms for these angiogenic alterations are largely unknown. Here we identify regulator of G-protein signalling 5 (*Rgs5*) as a master gene responsible for the abnormal tumour vascular morphology in mice. Loss of *Rgs5* results in pericyte maturation, vascular normalization and consequent marked reductions in tumour hypoxia and vessel leakiness. These vascular and intratumoral changes enhance influx of immune effector cells into tumour parenchyma and markedly prolong survival of tumour-bearing mice. This is the first demonstration, to our knowledge, of reduced tumour angiogenesis and improved immune therapeutic outcome on loss of a vascular gene function and establishes a previously unrecognized role of G-protein signalling in tumour angiogenesis.

During tumour-induced angiogenesis, the two important vascular cell types, endothelial cells and surrounding pericytes, develop multiple morphological and architectural abnormalities[7,8] as well as altered expression of marker proteins[9–12]. Using the RIP-Tag mouse model of pancreatic islet carcinogenesis (SV40 large T antigen expressed under the control of the rat insulin gene (*Ins2*) promoter), we have recently observed that *Rgs5* is overexpressed in the aberrant tumour vasculature[10].

Rgs5 is expressed by pericytes in the vascular bed and is the first marker for a subgroup of platelet-derived growth factor receptor β $(PDGFR\beta)^+$ progenitor perivascular cells that regulate vascular survival in tumours[8]. RGS molecules are a family of biochemically well-characterized molecules that inhibit signalling from G-protein-coupled receptors by stimulating the intrinsic GTPase activity of activated Gα proteins[13]. However, their function *in vivo* is largely unknown. *Rgs5* is constitutively expressed in a variety of organs, especially brain, heart, aorta, skeletal muscle, liver and kidney, and is also upregulated in RIP1-Tag5 tumour vessels[10,14].

To study the role of RGS5 in tumour angiogenesis and vascular normalization, we generated *Rgs5*-deficient mice by crossing recombinant mice harbouring a *loxP*-flanked *Rgs5* exon 1 with Cre-deleter mice. On exon 1 deletion, *Rgs5* expression is absent in heart, kidney, brain, lung and liver (Fig. 1a, b). *Rgs5*-deficient mice develop normally and present with no gross histological abnormalities. $Rgs5^{-/-}$ mice were intercrossed with transgenic RIP1-Tag5 mice to assess survival and intratumoral characteristics (Supplementary Fig. 1). RIP1-Tag5 mice develop tumours in a well-characterized sequence of events from normal Tag^+ islets to hyperplastic and angiogenic islets, and eventually form insulinomas, which cause premature death due to hypoglycaemia. Early tumorigenesis is unchanged in the $Rgs5^{-/-}$ background, as documented by a comparable number of angiogenic islets per mouse (Fig. 1c). At later tumour stages, the *Rgs5*-deficient background enhances tumour growth, as shown by an increase in overall tumour burden over age and premature death caused by hypoglycaemia (Fig. 1d). This is in agreement with the reduced survival of *Rgs5*-deficient RIP1-Tag5 mice compared to RIP1-Tag5 wild-type mice ($P < 0.0001$; range, 27 ± 3 weeks for RIP1-Tag5 × $Rgs5^{-/-}$, 30 ± 3 weeks for RIP1-Tag5; Fig. 1e).

To assess tumour vascular morphology, insulinomas in RIP1-Tag5 wild-type or *Rgs5*-deficient RIP1-Tag5 mice at 27 weeks of age were visualized after lectin perfusion using confocal microscopy (Fig. 2a–c). Notably, the vascular network in $Rgs5^{-/-}$ insulinomas resembles normal vessels with regard to vessel diameters and distribution (for overview, see Supplementary Fig. 2). This is in contrast with insulinomas in wild-type mice, which display a chaotic vascular architecture with large vessels adjacent to small vessels and a heterogeneous vessel density. This finding demonstrates that loss of *Rgs5* expression results in vessel normalization.

Because vascular *Rgs5* expression is restricted to pericytes, we hypothesized that pericyte maturation, abundance and/or attachment along the vessel wall is intimately associated with the observed vascular normalization. Pericyte coverage and association with endothelial cells were unchanged in *Rgs5*-deficient tumours (Supplementary Fig. 3). However, pericyte phenotypes differed between wild-type and *Rgs5*-deficient tumours. In RIP-Tag wild-type tumours, most pericytes are positive for both PDGFRβ and *Rgs5*, representing immature progenitor cells with the potential to differentiate into mature pericytes *in vitro*. A smaller subpopulation of mature pericytes that are immunoreactive for *NG2* (also known as *Cspg4*), desmin and *αSMA* (also known as *Acta2*) is also found in these tumours[8]. By contrast, *Rgs5*-deficient tumour pericytes in age- and size-matched tumour samples predominantly express αSMA and also NG2—recognized markers of maturity[8] (Fig. 2d, e). These data indicate that in the absence of *Rgs5*, tumour pericytes are of a more mature phenotype.

Diverse functions have been described for pericytes, ranging from haemodynamic regulation to vessel stability and permeability[15]. Because *Rgs5*-deficient mice display notably improved vascular integrity and maturity, we reasoned that concomitant changes in the tumour microenvironment were also likely. Interestingly, *Rgs5* expression has been shown to be increased under hydrostatic

[1]Western Australian Institute for Medical Research, UWA Centre for Medical Research, Perth, Western Australia 6000, Australia. [2]Juniorgroup Molecular Imaging, Department of Medical Physics in Radiology, [3]Department of Cellular and Molecular Pathology, and [4]Department of Molecular Immunology, German Cancer Research Center, 69120 Heidelberg, Germany. [5]Centre for Microscopy, Characterisation and Analysis, The University of Western Australia, Perth, Western Australia 6000, Australia. [6]Institute of Physiology and Pathophysiology, University of Heidelberg, 69120 Heidelberg, Germany.

pressure *in vitro*, underscoring a direct correlation between angiogenesis, intratumoral hydrostatic pressure and *Rgs5* expression[16]. We found oxygen supply to be improved in *Rgs5*-deficient tumours compared to wild-type tumours, as demonstrated by a reduced tumour hypoxia; this was visualized by the formation of pimonidazole adducts (Fig. 3a). This finding may contribute to a growth advantage for *Rgs5*-deficient tumours, resulting in poorer survival (Fig. 1e).

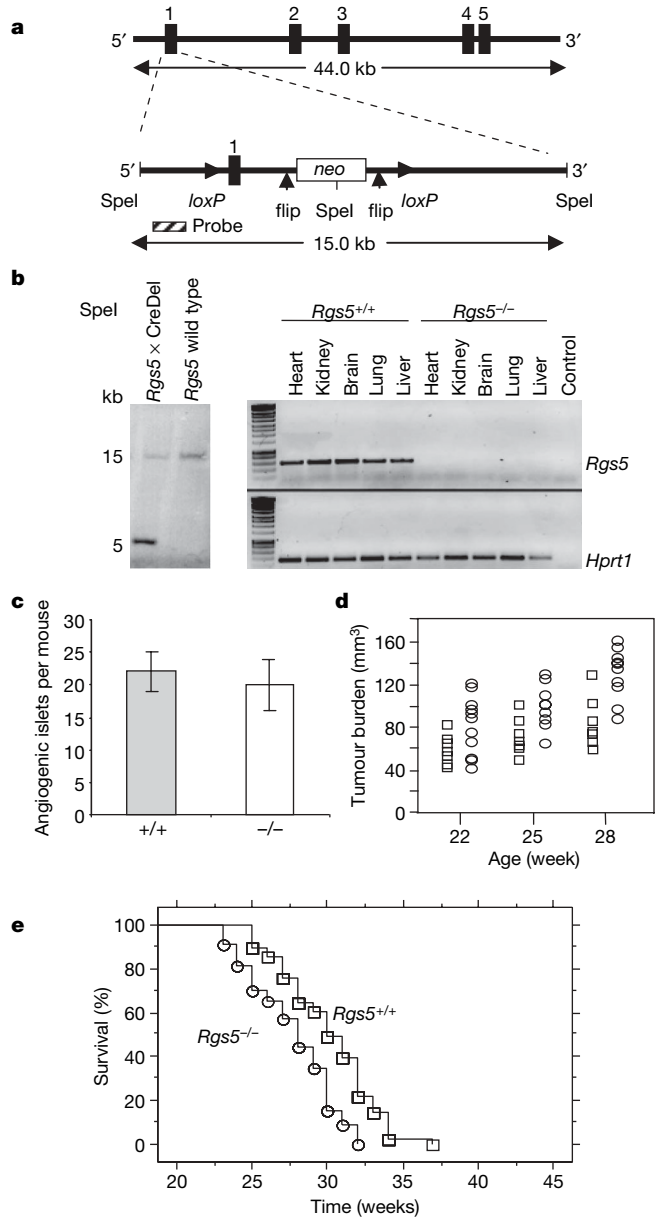

Figure 1 | Establishment of *Rgs5*$^{-/-}$ mice. **a**, *Rgs5* exon 1 was flanked with *loxP* sites, and a neomycin (*neo*) cassette was introduced into intron 1 and flanked by flip sites for removal after the selection process. SpeI restriction sites are shown. **b**, Left: Southern blot analysis of SpeI-digested tail DNA derived from F_1 offspring after crossbreeding with Cre-deleter (CreDel) mice and wild-type controls. Right: PCR with reverse transcription (RT–PCR) analysis of organs from a *Rgs5*$^{+/+}$ and a *Rgs5*$^{-/-}$ mouse. *Hprt1*, hypoxanthine phosphoribosyltransferase. **c**, The number of angiogenic islets in 18-week-old wild-type (grey bar) and *Rgs5*-deficient (white bar) RIP1-Tag5 mice ($n = 10$). Error bars represent s.e.m. **d**, Tumour burden in wild-type (open squares) and *Rgs5*-deficient (open circles) mice at the age of 22, 25 and 28 weeks ($n = 10$; range: *Rgs5*$^{+/+}$, 41–87 mm^3, 53–108 mm^3, 57–132 mm^3, respectively; *Rgs5*$^{-/-}$, 35–128 mm^3, 63–135 mm^3 and 82–166 mm^3, respectively). **e**, Kaplan–Meier survival analysis of RIP1-Tag5 wild-type (+/+, open squares, $n = 82$) and RIP1-Tag5 × *Rgs5*$^{-/-}$ mice (open circles, $n = 82$, $P < 0.0001$).

To evaluate further the physiological impact of vascular maturation, we compared vascular permeability of wild-type and *Rgs5*$^{-/-}$ tumours using dynamic contrast-enhanced magnetic resonance imaging (MRI) on 27-week-old mice. Notably, normalized tumour vessels in *Rgs5*$^{-/-}$ mice showed a 50% reduction in permeability for the contrast agent compared to wild-type RIP1-Tag5 tumours (Fig. 3b, $P = 0.008$). These are the first functional data demonstrating reduced leakiness of angiogenic vessels on loss of gene function *in vivo*. Thus, absence of *Rgs5* results in a reduced number of

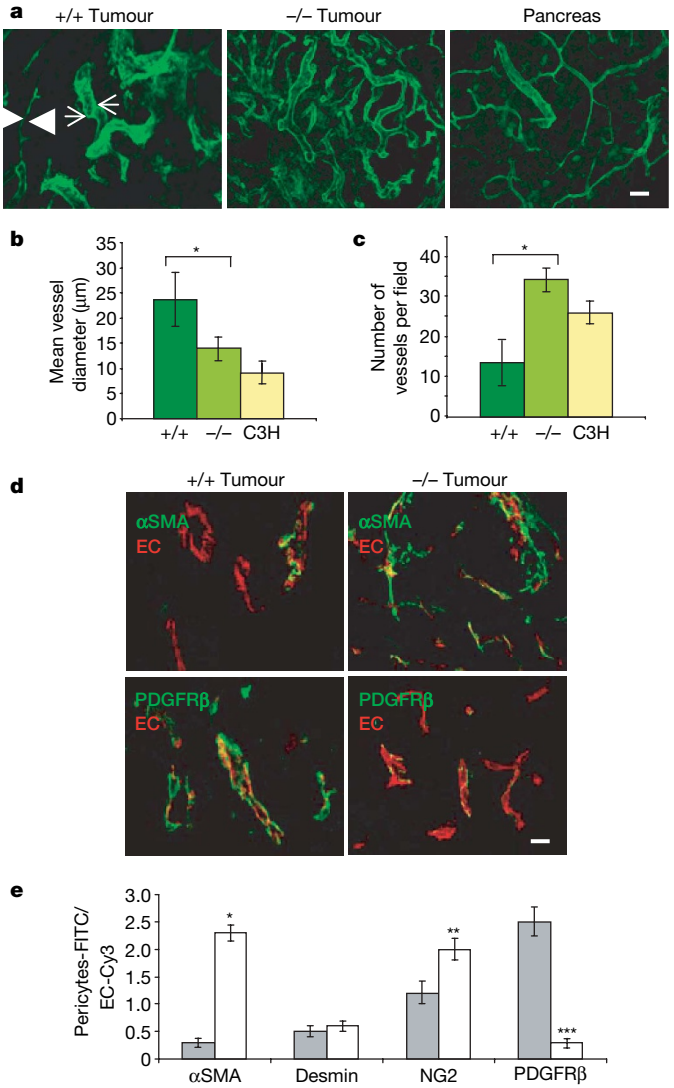

Figure 2 | Vascular normalization in *Rgs5*-deficient tumours. **a**, Confocal images of lectin-perfused vessels in RIP1-Tag5 wild-type (+/+, $n = 12$) and *Rgs5*-deficient (−/−, $n = 15$) size-matched tumours (40–65 mm^3), and C3H controls (pancreas; $n = 10$). Arrowheads point at a vessel with small caliber next to a vessel with large caliber (arrows). For these images, a ×20 objective was used; scale bar, 50 μm. **b**, Mean vessel diameters were quantified from wild-type (+/+) or *Rgs5*-deficient (−/−), size-matched tumours and C3H pancreatic tissue (C3H; 5 fields per tumour, 15 tumours, $^*P = 0.0009$). **c**, Vessel density within randomly selected fields excluding the tumour periphery (5 fields per tumour, 15 tumours, $^*P < 0.0001$). **d**, Confocal images from wild-type (+/+) and *Rgs5*-deficient (−/−) mice, labelled with anti-αSMA (green, upper panels) and anti-PDGFRβ (green, lower panels). Endothelial cells (EC) were stained with anti-CD31 (red). For these images, a ×60 objective was used; scale bar, 20 μm. **e**, Quantitative increase of the number of αSMA-, desmin-, NG2- and PDGFRβ-positive pericytes in wild-type (+/+, grey bars) and *Rgs5*-deficient (−/−, white bars) mice. The ratio of total area of green staining (pericyte markers) to red staining (EC) is provided (5 fields per tumour, 15 tumours, $^*P = 0.0001$, $^{**}P = 0.002$, $^{***}P = 0.0001$). All error bars represent s.e.m.

enlarged tumour vessels, increased oxygen supply to the tumour parenchyma and decreased tumour vascular permeability. These key findings were reproduced in a fibrosarcoma transplantation model (AG104A) that was subcutaneously grown in *Rgs5*-deficient mice (Supplementary Fig. 4). *Rgs5* is also a marker for developing pericytes in the brain[17], and its expression persists in adult brain vessels. We therefore investigated the role of RGS5 in the barrier function of brain capillaries during ischaemia. Interestingly, brain oedema after transient cerebral ischaemia was significantly reduced in *Rgs5*-deficient mice, demonstrating decreased permeability for plasma molecules in brain capillaries (Supplementary Table 1), and strongly supports our intratumoral findings (Fig. 3b).

Our previous work on RIP1-Tag5 tumour immunity showed a strong correlation between vascular remodelling induced by intratumoral inflammation and lymphocyte influx[5,18,19]. However, we did not know whether lymphocyte migration into tumour parenchyma was enhanced by vessel remodelling or by an ongoing local immune response. We sought to address this question by adoptively transferring *ex vivo* activated H–2^k-restricted anti-Tag $CD4^+$ and $CD8^+$ T cells into 27-week-old tumour-bearing RIP1-Tag5 × $Rgs5^{-/-}$ mice bred into the C3H background (H–2^k). Seven days after transfer (the peak of pre-activated Tag-specific T cell proliferation *in vivo*[19]), tumours were harvested and analysed. Untreated tumours in wild-type RIP1-Tag5 mice did not show a spontaneous T-cell infiltrate; by contrast, *Rgs5*-deficient mice consistently displayed a higher degree of spontaneous T-cell infiltration, although this did not reach statistical significance (Fig. 4a and Supplementary Fig. 5). Vessel wall inflammation or upregulation of cytokines and chemokines in untreated $Rgs5^{-/-}$ tumours were not observed. However, after adoptive transfer (total of 5×10^6 $CD4^+$ and $CD8^+$ T cells), tumours in the *Rgs5*-deficient mice were massively infiltrated by $CD8^+$ and $CD4^+$ T cells, whereas wild-type RIP1-Tag5 tumours showed no significant increase in infiltrating lymphocytes (Fig. 4a and Supplementary Fig. 5). Thus, *Rgs5* loss in angiogenic blood vessels 'opens' tumours for immune cell penetration—a very notable finding further substantiated by impressive survival in subsequent studies.

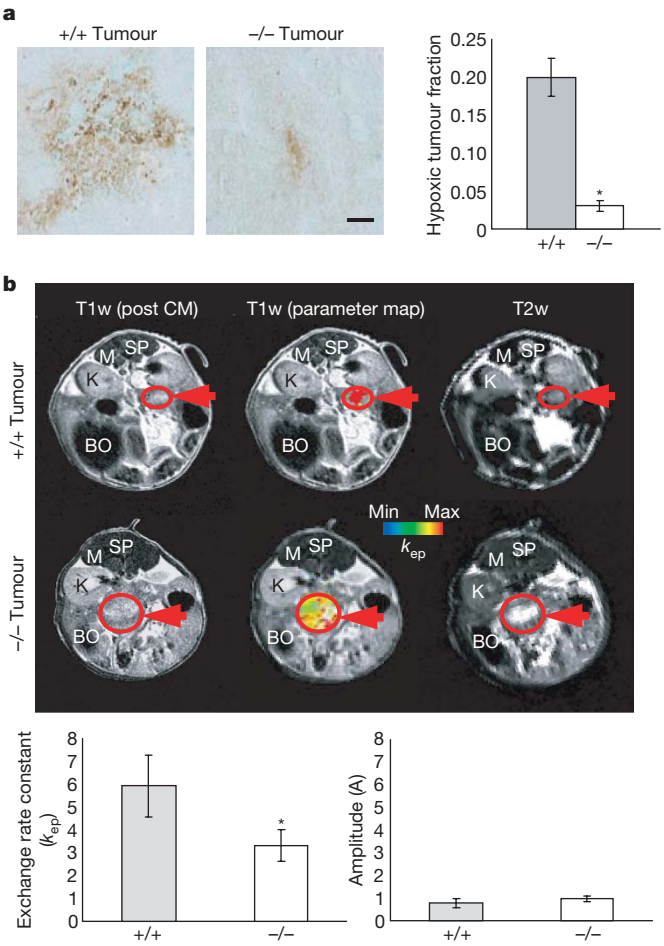

Figure 3 | Improved oxygenation and reduced vessel leakiness in *Rgs5*$^{-/-}$ tumours. a, Hypoxia in 27-week-old RIP1-Tag5 (+/+) and RIP1-Tag5 × $Rgs5^{-/-}$ (−/−) mice ($n = 20$ tumours, size matched, range of 40–65 mm^3, $P < 0.0001$). For these images, a ×20 objective was used; scale bar, 50 μm. Error bars represent s.e.m. **b**, Photographs represent T1-weighted (T1w; post CM, post contrast media) MRI images and the corresponding colour-coated parameter maps of the exchange rate constant k_{ep} (indicating vessel permeability), and T2-weighted MRI images of RIP1-Tag5 wild-type (+/+, upper panel) and RIP1-Tag5 × $Rgs5^{-/-}$ (−/−, lower panel) mice recorded with a 1.5 tesla (T) whole-body MR scanner in combination with a small animal coil. Arrows indicate location of tumours. BO, bowel; K, kidney; M, dorsal muscle; SP, spine. Graphs represent quantitative analyses of MRI studies (one-sided *t*-test): k_{ep}, exchange rate constant; A, amplitude indicating relative blood volume ($n = 10$, $^*P = 0.008$). Error bars represent s.d.

Cohorts of wild-type and *Rgs5*-deficient RIP1-Tag5 mice (23 weeks old with significant tumour burdens; average range, 50–120 mm^3) were adoptively transferred with *in vitro* activated $CD4^+$ and $CD8^+$ anti-Tag T cells in two-week intervals. In parallel, equal numbers of non-specifically (concanavalin A, ConA) activated or naive T cells from C3H control mice were transferred. As previously reported, adoptive transfer of activated, Tag-specific, naive or ConA-activated lymphocytes alone does not confer a survival advantage to RIP1-Tag5 mice[19,20], with the mice succumbing to insulinomas at 32 ± 2, 29 ± 2 and 29 ± 3 weeks of age, respectively (Fig. 4b–d). However, RIP1-Tag5 × $Rgs5^{-/-}$ recipients showed substantially prolonged survival after the transfer of pre-activated, Tag-specific T cells (age 41 ± 7 weeks, $P = 0.0004$; the experiment was terminated when surviving mice reached 48 weeks), correlating with the marked parenchymal influx of anti-Tag immune cells (Fig. 4a), although repeated T-cell infusions were required owing to their limited lifespan in a non-inflammatory tumour environment. This survival advantage is tumour-antigen-specific and requires activated anti-Tag T cells because no such effect was seen with transfer of ConA-activated or naive lymphocytes (survival: 28 ± 3 and 27 ± 3 weeks, respectively, Fig. 4c, d). Similarly, *Rgs5*-deficient mice are highly responsive to therapeutic anti-Tag vaccination (survival: 47 ± 7 weeks, $P < 0.0001$, started at 23 weeks); in contrast, vaccination strategies in wild-type RIP1-Tag5 mice are only successful in an early prophylactic setting before tumour development (starting at week 6, ref. 20), and fail later, when highly vascularized tumours are established (Fig. 4e and Supplementary Fig. 6).

The present study identifies RGS5 as a key regulator controlling the aberrant morphology of the tumour vasculature. Moreover, our results demonstrate the highly dynamic and reversible nature of tumour angiogenesis. Loss of *Rgs5* gene function induces notable morphological and physiological changes in the tumour vasculature and microenvironment. Importantly, deficiency of *Rgs5* reduces angiogenic activity and notably improves the outcome of specific therapeutic interventions.

This study has some overlapping features with anti-angiogenesis therapy in relation to vessel diameters and alleviation of hypoxia. Blocking vascular endothelial growth factor (VEGF) signalling in tumours has been shown to create a 'vascular normalization window' that decreases interstitial pressure and enhances tumour oxygenation and the therapeutic response to cytotoxic drugs and/or radiation in mouse and human cancers[21,22]. *Rgs5* deficiency is, however, clearly distinct with regard to vessel density and results in changes to intratumoral pericyte phenotype rather than pericyte coverage[23]. Furthermore, we show for the first time, to our knowledge, an association between vessel normalization in the absence of *Rgs5* and an increased anti-tumour immune response. Whereas VEGF-blocking therapies clearly enhance drug efficacy, correlating with changes in vascular morphology, pericyte maturation shown in this study may

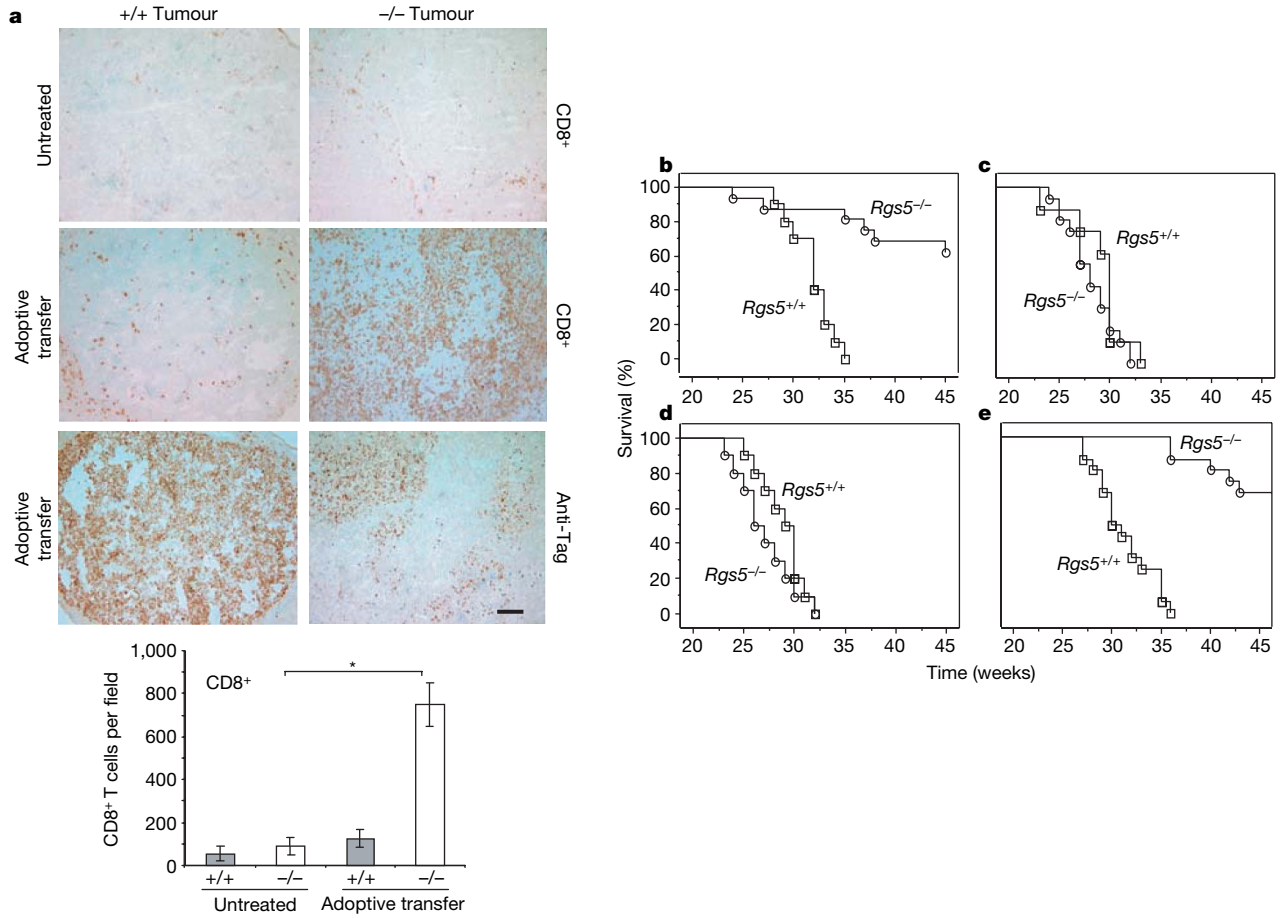

Figure 4 | Immune-mediated tumour rejection after vascular normalization. a, Spontaneous infiltration of $CD8^+$ immune cells measured in tumours of 27-week-old RIP1-Tag5 wild-type (+/+) and *Rgs5*-deficient (−/−) mice (upper images). Infiltration of $CD8^+$ T cells after adoptive transfer into 27-week-old RIP1-Tag5 wild-type and $Rgs5^{-/-}$ mice (middle images) and corresponding anti-Tag tumour staining (lower images). For these images, a ×10 objective was used; scale bar, 100 μm. The graph shows quantification of $CD8^+$ lymphocytic infiltration in size-matched RIP1-Tag5 wild-type (grey bars) and *Rgs5*-deficient (white bars) tumours without treatment and after adoptive transfer (5 fields per tumour, $n = 15$ tumours, $^*P < 0.0001$). Error bars represent s.e.m. **b–d**, Kaplan–Meier-survival studies on RIP1-Tag5 wild-type ($Rgs5^{+/+}$, open squares, $n = 10$–16) and RIP1-Tag5 × $Rgs5^{-/-}$ mice ($Rgs5^{-/-}$, open circles, $n = 12$–16) treated with: **b**, pre-activated anti-Tag T cells (logrank test, $P = 0.0004$); **c**, non-specific ConA-activated T cells ($P = 0.27$); or **d**, naive T cells from C3H mice ($P = 0.24$). Treatment start, 23 weeks; untreated controls are shown in Fig. 1e. **e**, Survival of RIP1-Tag5 wild-type (open square, $n = 16$) and *Rgs5*-deficient (open circle, $n = 16$) mice after vaccination with Tag and CpG-ODN 1668, $P < 0.0001$. Treatment start: 23 weeks.

also contribute to the anti-tumour effects by directly influencing leukocyte attachment and transmigration into tumour parenchyma. There is emerging evidence that resistance develops to anti-VEGF/VEGF receptor therapies, and that re-growth of treated tumours may occur due to compensation by other pro-angiogenic factors[24]. Here we provide novel mechanistic insights into reversing tumour angiogenesis independently of anti-angiogenic drugs by targeting G-protein signalling. Studies are under way to elucidate pathways regulated by RGS5 in tumour pericytes for pharmacotherapeutic intervention in combination with immune therapy. Recognition that RGS5 is a broadly expressed tumour antigen[25] and is also vessel-associated in numerous tumours (for example, astrocytomas and insulinomas[10], renal cell carcinoma[26] and hepatocellular carcinoma[27]) confirms its general importance in tumorigenesis and expands potential therapeutic opportunities.

METHODS SUMMARY

Rgs5-deficient mice were established by removing exon 1. $Rgs5^{-/-}$ mice were crossbred with RIP1-Tag5, SV40 large T antigen transgenic mice on a C3H background. Angiogenic islets and tumours were isolated from pancreatic tissue. Confocal microscopy was performed on lectin-perfused, albumin/gelatine-embedded, vibrotome-dissected tissue to assess vascular density and vessel diameters. Anti-αSMA, anti-PDGFRβ, anti-NG2 and anti-desmin histology was used to assess pericyte maturation. Hypoxia in islet tumours was detected by the formation of pimonidazole adducts after the injection of pimonidazole hydrochloride compound into tumour-bearing mice. MRI was performed using a 1.5 tesla whole-body MR-scanner (Siemens Symphony) in combination with a custom-made radio-frequency coil for excitation and signal reception to assay vascular leakiness. Anti-Tag, $CD4^+$ and $CD8^+$ transgenic T cells were used for adoptive transfers to evaluate lymphocyte access into tumours. Vaccination studies were performed using 50 μg of Tag protein mixed with 50 μg of CpG-oligodeoxynucleotide (ODN) 1668.

Full Methods and any associated references are available in the online version of the paper at www.nature.com/nature.

Received 14 December 2007; accepted 25 February 2008.
Published online 16 April 2008.

1. Hanahan, D. & Folkman, J. Patterns and emerging mechanisms of the angiogenic switch during tumorigenesis. *Cell* **86**, 353–364 (1996).
2. Ryschich, E., Schmidt, J., Hammerling, G. J., Klar, E. & Ganss, R. Transformation of the microvascular system during multistage tumorigenesis. *Int. J. Cancer* **97**, 719–725 (2002).
3. Heldin, C. H., Rubin, K., Pietras, K. & Ostman, A. High interstitial fluid pressure — an obstacle in cancer therapy. *Nature Rev. Cancer* **4**, 806–813 (2004).
4. Jain, R. K., Tong, R. T. & Munn, L. L. Effect of vascular normalization by antiangiogenic therapy on interstitial hypertension, peritumor edema, and lymphatic metastasis: insights from a mathematical model. *Cancer Res.* **67**, 2729–2735 (2007).
5. Ganss, R., Arnold, B. & Hammerling, G. J. Mini-review: overcoming tumor-intrinsic resistance to immune effector function. *Eur. J. Immunol.* **34**, 2635–2641 (2004).

6. Buckanovich, R. J. *et al.* Endothelin B receptor mediates the endothelial barrier to T cell homing to tumors and disables immune therapy. *Nature Med.* **14,** 28–36 (2008).
7. Morikawa, S. *et al.* Abnormalities in pericytes on blood vessels and endothelial sprouts in tumors. *Am. J. Pathol.* **160,** 985–1000 (2002).
8. Song, S., Ewald, A. J., Stallcup, W., Werb, Z. & Bergers, G. PDGFRβ^+ perivascular progenitor cells in tumours regulate pericyte differentiation and vascular survival. *Nature Cell Biol.* **7,** 870–879 (2005).
9. Benjamin, L. E., Golijanin, D., Itin, A., Pode, D. & Keshet, E. Selective ablation of immature blood vessels in established human tumors follows vascular endothelial growth factor withdrawal. *J. Clin. Invest.* **103,** 159–165 (1999).
10. Berger, M., Bergers, G., Arnold, B., Hammerling, G. J. & Ganss, R. Regulator of G-protein signaling-5 induction in pericytes coincides with active vessel remodeling during neovascularization. *Blood* **105,** 1094–1101 (2005).
11. Ryschich, E. *et al.* Molecular fingerprinting and autocrine growth regulation of endothelial cells in a murine model of hepatocellular carcinoma. *Cancer Res.* **66,** 198–211 (2006).
12. Seaman, S. *et al.* Genes that distinguish physiological and pathological angiogenesis. *Cancer Cell* **11,** 539–554 (2007).
13. Hollinger, S. & Hepler, J. R. Cellular regulation of RGS proteins: modulators and integrators of G protein signaling. *Pharmacol. Rev.* **54,** 527–559 (2002).
14. Chen, C., Zheng, B., Han, J. & Lin, S. C. Characterization of a novel mammalian RGS protein that binds to Gα proteins and inhibits pheromone signaling in yeast. *J. Biol. Chem.* **272,** 8679–8685 (1997).
15. Allt, G. & Lawrenson, J. G. Pericytes: cell biology and pathology. *Cells Tissues Organs* **169,** 1–11 (2001).
16. Manome, Y., Saeki, N., Yoshinaga, H., Watanabe, M. & Mizuno, S. A culture device demonstrates that hydrostatic pressure increases mRNA of RGS5 in neuroblastoma and CHC1-L in lymphocytic cells. *Cells Tissues Organs* **174,** 155–161 (2003).
17. Bondjers, C. *et al.* Transcription profiling of platelet-derived growth factor-B-deficient mouse embryos identifies RGS5 as a novel marker for pericytes and vascular smooth muscle cells. *Am. J. Pathol.* **162,** 721–729 (2003).
18. Ganss, R. & Hanahan, D. Tumor microenvironment can restrict the effectiveness of activated antitumor lymphocytes. *Cancer Res.* **58,** 4673–4681 (1998).
19. Ganss, R., Ryschich, E., Klar, E., Arnold, B. & Hammerling, G. J. Combination of T-cell therapy and trigger of inflammation induces remodeling of the vasculature and tumor eradication. *Cancer Res.* **62,** 1462–1470 (2002).
20. Garbi, N., Arnold, B., Gordon, S., Hammerling, G. J. & Ganss, R. CpG motifs as proinflammatory factors render autochthonous tumors permissive for infiltration and destruction. *J. Immunol.* **172,** 5861–5869 (2004).
21. Jain, R. K. Normalization of tumor vasculature: an emerging concept in antiangiogenic therapy. *Science* **307,** 58–62 (2005).
22. Batchelor, T. T. *et al.* AZD2171, a pan-VEGF receptor tyrosine kinase inhibitor, normalizes tumor vasculature and alleviates edema in glioblastoma patients. *Cancer Cell* **11,** 83–95 (2007).
23. Winkler, F. *et al.* Kinetics of vascular normalization by VEGFR2 blockade governs brain tumor response to radiation: role of oxygenation, angiopoietin-1, and matrix metalloproteinases. *Cancer Cell* **6,** 553–563 (2004).
24. Casanovas, O., Hicklin, D. J., Bergers, G. & Hanahan, D. Drug resistance by evasion of antiangiogenic targeting of VEGF signaling in late-stage pancreatic islet tumors. *Cancer Cell* **8,** 299–309 (2005).
25. Boss, C. N. *et al.* Identification and characterization of T-cell epitopes deduced from RGS5, a novel broadly expressed tumor antigen. *Clin. Cancer Res.* **13,** 3347–3355 (2007).
26. Furuya, M. *et al.* Expression of regulator of G protein signalling protein 5 (RGS5) in the tumour vasculature of human renal cell carcinoma. *J. Pathol.* **203,** 551–558 (2004).
27. Chen, X. *et al.* Novel endothelial cell markers in hepatocellular carcinoma. *Mod. Pathol.* **17,** 1198–1210 (2004).

Supplementary Information is linked to the online version of the paper at www.nature.com/nature.

Acknowledgements We thank G. Küblbeck, A. Klevenz, G. Hollman and S. Schmidt for technical support in establishing *Rgs5*-knockout mice, K. Bieber for assessing brain ischaemia, B. Misselwitz for providing the contrast agent Gadomer, and H. Ee and G. Bergers for critical reading of the manuscript. This study was supported by a National Health and Medical Research Council of Australia Project Grant, start-up funds from the Western Australian Institute for Medical Research and University of Western Australia (to R.G.), the Deutsche Forschungsgemeinschaft, and the EU projects MUGEN and CancerImmunoTherapy. Microscopy was carried out using facilities at the Centre for Microscopy and Microanalysis/Biomedical Image and Analysis Facility, The University of Western Australia, which are supported by University, State and Federal Government funding.

Author Contributions J.H. and M.M. performed animal experiments and histology, and analysed data; M.J. and F.K. performed MRI analyses; P.R. performed confocal microscopy studies; H.H.M and T.R. coordinated and analysed brain infarct experiments; S.K. and H.-J.G. performed electron microscopy; G.J.H. and B.A. contributed to the design of *Rgs5*-knockout studies; and R.G. designed and performed experiments, coordinated all studies and wrote the manuscript.

Author Information Reprints and permissions information is available at www.nature.com/reprints. Correspondence and requests for materials should be addressed to R.G. (ganss@waimr.uwa.edu.au).

METHODS

Mice and cells lines. RIP1-Tag5 mice (on a C3H background, provided by D. Hanahan) express the oncogene Tag under the control of the rat insulin gene promoter (RIP) in pancreatic β cells, and develop spontaneous tumours. In RIP1-Tag5 mice, Tag is expressed in adult mice at around week 8 to 10. Knockout mice were generated on a mixed (129 × C57BL/6) background and subsequently crossed with RIP1-Tag5/C3H mice for 8 generations. Although crossings continued up to generation 12, mice from generation 8 onwards (RIP1-Tag5 × *Rgs5*$^{+/-}$) were intercrossed with *Rgs5*$^{+/-}$ littermates to obtain larger cohorts of RIP1-Tag5 wild-type (+/+) and *Rgs5*-deficient (−/−) RIP1-Tag5 mice. For adoptive transfer experiments, mice transgenic for a T-cell receptor (TCR) that recognizes Tag presented by the MHC class I molecule H–2K^{k} (referred to as TCRCD8, provided by T. Geiger and R. Flavell) or by the MHC class II molecule I-A (TagTCR1, provided by I. Förster) were used on a C3H background as previously described[20]. All experimental protocols were approved by the Animal Welfare Board of the Regierungspräsidium Karlsruhe, Germany, or the Animal Ethics Committee of the University of Western Australia. AG104A cells, a spontaneous fibrosarcoma of C3H mice (provided by H. Schreiber), were injected subcutaneously (5×10^5 cells) into C3H or *Rgs5*-deficient C3H mice.

Determination of the number of angiogenic islets and tumour burden. Angiogenic islets were isolated by retrograde perfusion after collagenase digestion. Islets with visible haemorrhaging were counted as angiogenic islets under a dissecting microscope. Tumours were microdissected from freshly excised pancreata. Tumour volumes were measured with callipers, and the formula volume = 0.52 × width^2 × length for approximating the volume of a spheroid was applied.

Antibodies and histological analyses. Sections were stained with the following antibodies: anti-CD4 (rat, GK1.5, 10 μg ml^{-1}, BD PharMingen), anti-CD8 (rat, Ly-2, 10 μg ml^{-1}, BD PharMingen) and anti-Tag (rabbit polyclonal, 1:1,000, from D. Hanahan), followed by anti-rat or anti-rabbit biotinylated secondary reagents (Vector Laboratories). Anti-CD31 (rat IgG2a, MEC 13.3, 5 μg ml^{-1}, BD PharMingen) and anti-PDGFRβ (rat IgG2, 10 μg ml^{-1}, eBioscience) staining was followed by cyanin 3 (Cy3) or FITC (fluorescein isothiocyanate)-conjugated IgG F(ab′)$_2$ fragment goat anti-rat (3 μg ml^{-1}, Dianova) as the secondary reagent. Anti-NG2 (rabbit anti-mouse, 1:500, Chemikon) staining was followed by FITC-conjugated IgG immunoglobulin donkey anti-goat (3 μg ml^{-1}, Dianova) as secondary reagent. Stainings for anti-αSMA (mouse IgG1, 5 μg ml^{-1}, Sigma) and anti-desmin (mouse IgG1, D33, 1:300, Dako) were performed using the FITC–MOM kit (Vector). The hypoxyprobe-1 kit (Chemicon) was used to detect hypoxia. Hypoxic tumour area was quantified throughout tumours on sections that were 100 μm apart. For assessment of immune infiltration, standard histology[19] was performed 7 days after T-cell transfer. Tumour sections were evaluated for CD4$^+$/CD8$^+$ lymphocytic infiltration by using a ×20 objective lens, and five independent areas were selected, digitally photographed and counted (ImagePro). Tumour tissue was counterstained with methyl green. *In situ* hybridization is described elsewhere[10].

Dynamic magnetic resonance imaging and vascular permeability. MRI was performed using a 1.5 tesla whole-body MR-scanner (Siemens Symphony) in combination with a custom-made radio-frequency coil for excitation and signal reception. Morphologic MR-imaging was performed using a transversal T2-weighted turbo-spin echo sequence (repetition time, TR = 1,510 ms, echo time, TE = 59 ms, field of view, FOV = 50 × 50 mm^2, matrix = 128, slice thickness = 1.0 mm). Kinetics of the contrast agent in tumours were recorded using a T1-weighted inversion-recovery Turbo FLASH (IRTF) sequence (TR = 13 ms, TE = 5.3 ms, TI = 300 ms, slice thickness = 2 mm, FOV = 60 × 60 mm^2, Matrix 128). In total, 120 dynamic scans were acquired from two sections within 15.36 min. Five seconds after starting the dynamic contrast-enhanced magnetic resonance imaging (DCE-MRI) measurement, 100 μl (0.1 mmol per kg body weight) of the paramagnetic contrast agent Gadomer (Bayer-Schering Pharma) were injected manually within 5 s into the tail vein. Data were analysed using the pharmacokinetic two-compartment model of Brix, providing the parameters Amplitude (related to relative blood volume) and exchange rate constant k_{ep} (surrogate marker of vessel permeability)[28]. Vascular permeability in AG104A mice was determined using Evans blue as described[24] with minor modifications. Evans blue (Sigma) was intravenously injected into tumour-bearing mice on day 15 at 20 mg kg^{-1}. Fifteen minutes later, mice were perfused with PBS, tissues excised, and Evans blue extracted from tissue for 24 h at room temperature (23°C).

Confocal laser scanning microscopy. Mice were injected intravenously with 100 μg of FITC-labelled tomato lectin (from *Lycopersicon esculentum*, Vector Laboratories) in PBS. After 3 min of circulation, mice were heart-perfused with 4% paraformaldehyde in PBS. Organs were embedded in 36% albumin/3% gelatine, and 200-μm sections were cut with a vibratome and analysed with a Biorad MRC 1000/1024 ultraviolet confocal microscope using a Nikon UV-F ×20, NA 0.8 glycerine immersion objective or a Nikon PlanApo ×60, NA 1.4 oil immersion objective. Images were processed by using Photoshop 8.0 (Adobe Systems).

Transmission electron microscopy. For electron microscopy, tumours were fixed in 4% PFA and embedded in araldite. Ultrathin sections (70 nm) were cut on an ultracut UCT Leica microtome. Sections were contrasted with uranyl-acetate and lead citrate, and analysed with an EM 900 Zeiss electron microscope.

Brain ischaemia. Transient cerebral ischaemia was introduced using the intraluminal filament technique[29]. In adult mice, the left middle cerebral artery was occluded with an 8-0 nylon filament under anaesthesia. Ninety minutes after the ischaemic insult, the filament was withdrawn. Twenty-four hours after reperfusion, the brain was removed and sections stained with silver nitrate. Normal tissue is darkly stained by silver nitrate whereas the damaged area appears bright. The infarct and oedema volumes were calculated as described[30] by comparing the noninfarcted right hemisphere with the left hemisphere.

Adoptive transfers and vaccination studies. TCRCD8 splenocytes or TagTCR1 lymph node cells were activated *in vitro* for 3 days with 10 U of recombinant human IL-2 per ml, and 25 mM Tag peptide 362–568 (SEFLIEKRI for TCRCD8 cells) or 25 nM Tag peptide 362–384 (TNRFNDLLDRMDIMFGSTGSADI for TagTCR1 cells). C3H-derived splenocytes were activated with 1 μg ml^{-1} Con A (Sigma). 2.5×10^6 naive or activated CD4$^+$ and 2.5×10^6 CD8$^+$ T cells were transferred. Tag was purified from High Five insect cells infected with a baculovirus expressing the SV40 early region. Mice were primed with a single subcutaneous injection (tail base) of 50 μg Tag protein mixed with 50 μg CpG-ODN 1668 (phosphothioate-stabilized CpG-ODN 1668, TCCATGACGTTCCTGATGCT) in 200 μl PBS. Thereafter, CpG-ODN treatment groups were intraperitoneally injected with 50 μg Tag protein mixed with 50 μg CpG-ODN 1668 every second week.

Statistical analyses. Student's *t* test (two-tailed) was used unless otherwise indicated. $P < 0.05$ was considered to be statistically significant.

28. Brix, G. *et al.* Pharmacokinetic parameters in CNS Gd-DTPA enhanced MR imaging. *J. Comput. Assist. Tomogr.* **15,** 621–628 (1991).
29. Hata, R. *et al.* A reproducible model of middle cerebral artery occlusion in mice: hemodynamic, biochemical, and magnetic resonance imaging. *J. Cereb. Blood Flow Metab.* **18,** 367–375 (1998).
30. Lin, T. N., He, Y. Y., Wu, G., Khan, M. & Hsu, C. Y. Effect of brain edema on infarct volume in a focal cerebral ischemia model in rats. *Stroke* **24,** 117–121 (1993).